ACS OMEGA

Article

Cite This: ACS Omega 2019, 4, 15721−15728

http://pubs.acs.org/journal/acsodf

Identifying the Origins of Vacancies in the Crystal Structures of Rock Salt-type Chalcogenide Superconductors

Jasmin Simons and Simon Steinberg*

Institute of Inorganic Chemistry, RWTH Aachen University, Landoltweg 1, D-52074 Aachen, Germany

ABSTRACT: The tailored (computational) design of materials addressing future challenges requires a thorough understanding of their electronic structures. This becomes very apparent for a given material existing in a certain homogeneity range, as its particular composition influences its electronic structure and, eventually, its physical properties. This led us to explore the influence and, furthermore, the origin of vacancies in the crystal structures of rock salt-type superconductors by means of quantum-chemical techniques. In doing so, we examined the vibrational properties, electronic band structures, and nature of bonding for a series of superconducting transition-metal sulfides, i.e., MS (M = Sc, Y, Zr, Lu), which were identified to exist over certain homogeneity ranges. The outcome of our research indicates that the subtle competing interplay between two electronically unfavorable situations at the Fermi levels, i.e., the occupations of flat bands and the populations of antibonding states, appears to control the presence of vacancies in the crystal structures of the sulfides.

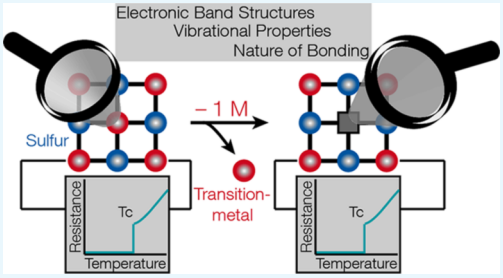

INTRODUCTION

To date, the full understanding of superconductivity has posed a challenge for chemists as well as physicists.[1] Even after the first conceptions[2,3] had provided adequate explanations for this phenomenon, the discoveries[4] of unanticipated superconducting states in cuprates have raised further questions and, hence, induced massive explorative efforts. To account for the findings of superconductivity in cuprates, considerable attention was paid to the influence of electron spectrum instabilities ("singularities"), which are located at the Fermi levels of superconductors.[5,6] Namely, the aforementioned electron spectrum instabilities are assumed to induce a structural distortion, which is counterbalanced by electrons residing in steep bands ("flat band/steep band scenario").[7,8] The latter idea[7] implies that the occurrence of a superconducting state tends to be linked to the presence of a flat band at the Fermi level in a given material. In this context, one may also consider that a particular composition could affect the position of a flat band relative to the Fermi levels in a given series of isostructural compounds, as atomic substitutions and/or structural defects influence the chemical compositions and, furthermore, the electronic (band) structures within such a set of materials.[9] Indeed, previous[10,11] temperature-dependent electric resistance measurements for series of isostructural compounds revealed that metal-to-superconductor transitions are observed solely for those species for which singularities are "pinned" to the Fermi levels.

Besides atomic substitutions,[12,13] structural defects ("vacancies") also influence the chemical compositions, electronic band structures, and, ultimately, the physical properties of compounds existing over certain homogeneity ranges. For instance, previous research[14−16] on cuprates forming over certain homogeneity ranges showed that the presence and, furthermore, temperatures of metal-to-superconductor transitions are linked to the amounts of oxygen vacancies in the crystal structures. Another series of superconductors, which form over certain homogeneity ranges, has been identified for chalcogenides crystallizing with the rock salt-type structure.[17,18] More recent research[19] on the electronic band structures of such rock salt-type chalcogenides based on initial, defect-free structure models revealed that flat bands were located near, but not at the Fermi levels in several of these compounds. In the flat band/steep band scenario,[7,8] such an outcome suggested an absence of metal-to-superconductor transitions being in stark contrast to the experimentally determined[17,18] results. This apparent discrepancy was explained by additional investigations showing that the locations of flat bands relative to the Fermi levels ought to be manipulated by the presence of vacancies in the crystal structures of these chalcogenides. But, what are the driving forces to crystallize with compositions that are related to vacancies in the crystal structures of the respective rock salt-type chalcogenides? To answer this question, we sought to investigate the electronic as well as vibrational properties, and the nature of bonding for a series of prototypical chalcogenide superconductors, i.e., MS (M = Sc, Y, Zr, Lu). In this contribution, we present the results of our explorations.

COMPUTATIONAL DETAILS

To provide an insight into the origins of the structural defects in chalcogenide superconductors, the electronic and vibrational features of four prototypical rock salt-type superconductors, that is, MS (M = Sc, Y, Zr, Lu), were examined. In addition to

Received: July 28, 2019
Accepted: August 30, 2019
Published: September 13, 2019

DOI: 10.1021/acsomega.9b02368
ACS Omega 2019, 4, 15721−15728

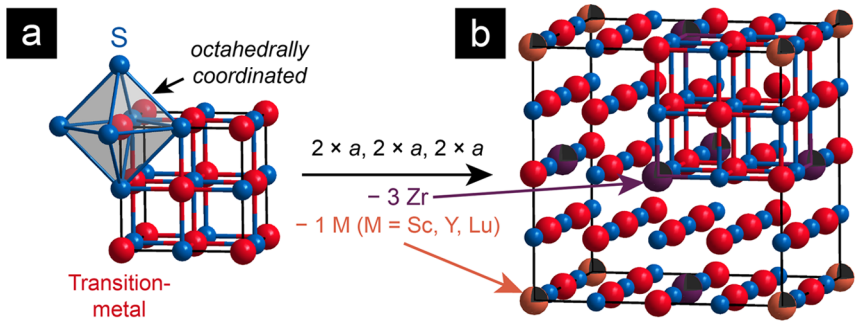

Figure 1. Representations of the crystal structures of (a) the rock salt-type MS (M = Sc, Y, Zr, Lu) and (b) the metal-deficient structure models $M_{31}S_{32} \equiv M_{0.97}S$ (M = Sc, Y, Lu) and $Zr_{29}S_{32} \equiv Zr_{0.91}S$. The structure models of $M_{31}S_{32}$ and $Zr_{29}S_{32}$ are derived from those of MS (M = Sc, Y, Zr, Lu), as the unit cells of $M_{31}S_{32}$ and $Zr_{29}S_{32}$ correspond to 2 × 2 × 2 expansions of the unit cells related to MS (M = Sc, Y, Zr, and Lu). In the cases of $M_{31}S_{32}$, one transition-metal atom has been removed, while three zirconium atoms have been eliminated, leading to the $Zr_{29}S_{32}$ model.

the quantum-chemical computations for MS (M = Sc, Y, Zr, Lu), the electronic and vibrational properties were also explored for metal-deficient structure models, i.e., $M_{31}S_{32}$ (M = Sc, Y, Lu) and $Zr_{29}S_{32}$, which were generated based on 2 × 2 × 2 expansions of the unit cells of MS (M = Sc, Y, Zr, Lu). To provide greater insight into the vibrational properties of the zirconium-containing sulfides, the vibrational properties were also examined for Zr_3S_4, which has been previously reported[20] to crystallize with a superstructure of the respective rock salt-type sulfide. The compositions of the aforementioned, metal-deficient structure models were chosen considering the experimentally determined phase widths of the superconducting sulfides, which have been reported elsewhere.[17,18] Full structural optimizations, which included lattice parameters and atomic positions, were carried out for all materials using the projector-augmented wave method[21] as implemented in the Vienna ab initio simulation package[22−26] (VASP). Correlation and exchange in all computations were described by the generalized gradient approximation of Pedrew, Burke, and Ernzerhof,[27] and the energy cutoff of the plane wave basis sets was 500 eV. In the cases of the electronic band structure computations of constituting elements, i.e., Sc, Y, Lu, Zr, and S, sets of up to 16 × 16 × 16 *k*-points were used, while sets of 16 × 16 × 16 and 8 × 8 × 8 *k*-points were employed for MS (M = Sc, Y, Zr, Lu) and $M_{31}S_{32}$ (M = Sc, Y, Lu), $Zr_{29}S_{32}$, and Zr_3S_4, respectively. All computations were considered to have converged as the energy difference between two iterative steps fell below 10^{-8} (and 10^{-6}) eV/cell for the electronic (and ionic) relaxations. The coordinates of the high-symmetry *k*-paths within the Brillouin zones were generated utilizing the AFLOW[28] code, and the electronic band structures of all sulfides were visualized with the aid of the Python Materials genomics[29] (pymatgen) program.

The vibrational properties of MS (M = Sc, Y, Zr, Lu), $M_{31}S_{32}$ (M = Sc, Y, Lu), $Zr_{29}S_{32}$, and Zr_3S_4 were examined using the Parlinski−Li−Kawazoe[30] method as implemented in the Phonopy[31] code. In this approach, the phonon frequencies are determined based on force constant matrices, after the corresponding sets of the interatomic forces have been computed within supercells, in which a particular atom had been elongated. The interatomic forces were calculated using VASP in the Γ-point approximation, an approach that has largely been employed elsewhere.[32−34] The supercells employed in the computations corresponded to 4 × 4 × 4 and 2 × 2 × 2 expansions of the structurally optimized unit cells of MS (M = Sc, Y, Zr, Lu) and $M_{31}S_{32}$ (M = Sc, Y, Lu), Zr_3S_4 as well as $Zr_{29}S_{32}$, respectively.

Chemical bonding analyses for MS (M = Sc, Y, Zr, Lu), $M_{31}S_{32}$ (M = Sc, Y, Lu), and $Zr_{29}S_{32}$ were accomplished based on the crystal orbital Hamilton populations (COHP) and their respective integrated values. In the framework of the COHP[35,36] technique, the off-site projected densities-of-states (DOS) are weighted with the respective Hamilton matrix elements to indicate bonding, nonbonding, and antibonding interactions. Herein, the projected crystal orbital Hamilton population (pCOHP) technique,[37] which is a variant of the COHP method, has been employed. Namely, the Hamilton-weighted populations had to be projected from the outcome of the plane-wave-based calculations with the aid of the Local Orbital Basis Suite Towards Electronic Structure Reconstruction program (LOBSTER[35,37−39]) because the crystal orbitals, which are employed in the COHP procedure, are constructed from local basis sets. The representations of the densities-of-states (DOS) as well as pCOHP curves were plotted using the wxDragon[40] code.

RESULTS AND DISCUSSION

To understand the causes of the structural defects in rock salt-type superconductors at the atomic scale, the vibrational properties, the electronic structures, and the nature of bonding were explored for a series of superconducting sulfides, for which certain homogeneity ranges have been determined. In this context, the superconducting MS (M = Sc, Y, Zr, Lu) were chosen for the examinations because previous explorations[17,18,41−43] on the existence ranges of the sulfides revealed phase widths of $0.07 \geq x \geq 0$, $0.05 \geq x \geq -0.07$, $0.34 \geq x \geq -0.11$, and $0.17 \geq x \geq -0.33$ for the superconducting, NaCl-type $Sc_{1-x}S$, $Y_{1-x}S$, $Zr_{1-x}S$, and $Lu_{1-x}S$, respectively. Furthermore, it should be noted that additional explorations identified even metal-poorer sulfides, i.e., Sc_2S_3,[44] Lu_3S_4,[45] and Zr_3S_4,[43] whose crystal structures were determined to be superstructures of those corresponding to the NaCl-type sulfides.

Also, understanding the origins of the structural defects in the aforementioned sulfides at the atomic scale requires to reveal the dissimilarities between the electronic and vibrational properties of MS (M = Sc, Y, Zr, Lu) and those of sulfides that are metal-poorer relative to the former. To do so, the phonon band structures, electronic band structures, and crystal orbital Hamilton populations (COHP) were examined for MS (M = Sc, Y, Zr, Lu) and metal-deficient models whose crystal

DOI: 10.1021/acsomega.9b02368
ACS Omega 2019, 4, 15721−15728

Table 1. Quantum-Chemically Computed Enthalpies of Formation, ΔH_f, for MS (M = Sc, Y, Zr, Lu), $M_{31}S_{32}$, and $Zr_{29}S_{32}$[a,b]

compound	ΔH_f (kJ/mol)	compound	ΔH_f (kJ/mol)	ΔH_f ($M_{32}S_{32}$) − [ΔH_f ($M_{31}S_{32}$) + ΔH_f (M)] (kJ/mol)
ScS ≡ $Sc_{32}S_{32}$	−11 618.97	$Sc_{0.97}S$ ≡ $Sc_{31}S_{32}$	−11 520.12	499.59
YS ≡ $Y_{32}S_{32}$	−12 466.07	$Y_{0.97}S$ ≡ $Y_{31}S_{32}$	−12 359.59	514.24
ZrS ≡ $Zr_{32}S_{32}$	−8422.59	$Zr_{0.91}S$ ≡ $Zr_{29}S_{32}$	−8542.75	2573.95
LuS ≡ $Lu_{32}S_{32}$	−11 521.80	$Lu_{0.97}S$ ≡ $Lu_{31}S_{32}$	−11 496.90	404.83

[a]The enthalpies of formation of MS (M = Sc, Y, Zr, Lu) have been calculated for $M_{32}S_{32}$ (see the main text). [b]In the case of the zirconium-containing species, ΔH_f ($Zr_{29}S_{32}$) and three ΔH_f (Zr) were subtracted from ΔH_f ($Zr_{32}S_{32}$).

structures were generated based on those of MS (M = Sc, Y, Zr, Lu). More precisely, the unit cells of the models that are metal-deficient relative to MS (M = Sc, Y, Zr, Lu) correspond to 2 × 2 × 2 expansions of the unit cells of MS (M = Sc, Y, Zr, Lu) (Figure 1), but comprise one (and three) metal atoms less per cell for M = Sc, Y, Lu, (and Zr), respectively. Accordingly, the stoichiometry corresponding to a given metal-deficient model (Table 1) is located within the experimentally determined homogeneity range (see above) of the respective superconducting sulfide. To provide an insight into the stability trends for MS (M = Sc, Y, Zr, Lu), $M_{31}S_{32}$ (M = Sc, Y, Lu), and $Zr_{29}S_{32}$, we first inspected the respective enthalpies of formation and phonon band structures of the diverse sulfides.

Enthalpies of Formation and Phonon Band Structures. The enthalpies of formation at zero temperature were calculated based on the total (electronic ground state) energies because the pressure-dependent zero-temperature enthalpy, i.e., $H_{el}(p) = E_{el}(V(p)) + pV(p)$, approaches E_{el} as the pressure vanishes.[46,47] In this context, it should also be mentioned that this approach could be used since E_{el} approximates the internal energy at zero temperature.[47] Thus, the enthalpies of formation of MS (M = Sc, Y, Zr, Lu), $M_{31}S_{32}$ (M = Sc, Y, Lu), and $Zr_{29}S_{32}$ were computed by subtracting the sum of the total energies of all constituting elements from the total energy of the respective sulfide

$$\Delta H_f\ (M_{32}S_{32}) = [E_{el}\ (MS) - (E_{el}\ (M) + E_{el}\ (S))]\cdot 32$$

and

$$\Delta H_f\ (M_{31}S_{32}) = E_{el}\ (M_{31}S_{32}) - (31\cdot E_{el}\ (M) + 32\cdot E_{el}\ (S))$$

for p = 0 bar and T = 0 K. Notably, the enthalpy of formation of the zirconium-deficient sulfide has been calculated based on total energies of $Zr_{29}S_{32}$ and 29 zirconium atoms. A comparison of the enthalpies of formation for all sulfides reveals negative values of ΔH_f for all materials such that the formations of these compounds tend to be preferred. Because the differences between ΔH_f ($M_{32}S_{32}$) and ΔH_f ($M_{31}S_{32}$), which have been evaluated according to

$$\Delta H_R = \Delta H_f\ (M_{32}S_{32}) - (\Delta H_f\ (M_{31}S_{32}) + \Delta H_f\ (M))$$

are positive for all inspected sulfides, one may infer that the formations of the metal-deficient species are preferred (note that enthalpies of formation of $Zr_{29}S_{32}$ and three zirconium atoms have been used in the case of the zirconium-containing sulfides).

An examination of the phonon band structures and densities-of-states for MS and $M_{31}S_{32}$ (M = Sc, Y, Lu; Figure 2) reveals that no negative values of the wavenumbers are evident for these sulfides. Because the presence of negative values of the phonon frequencies is typically indicative of a dynamic instability for a given material,[46] it can be concluded that MS and $M_{31}S_{32}$ (M = Sc, Y, Lu) are dynamically stable.

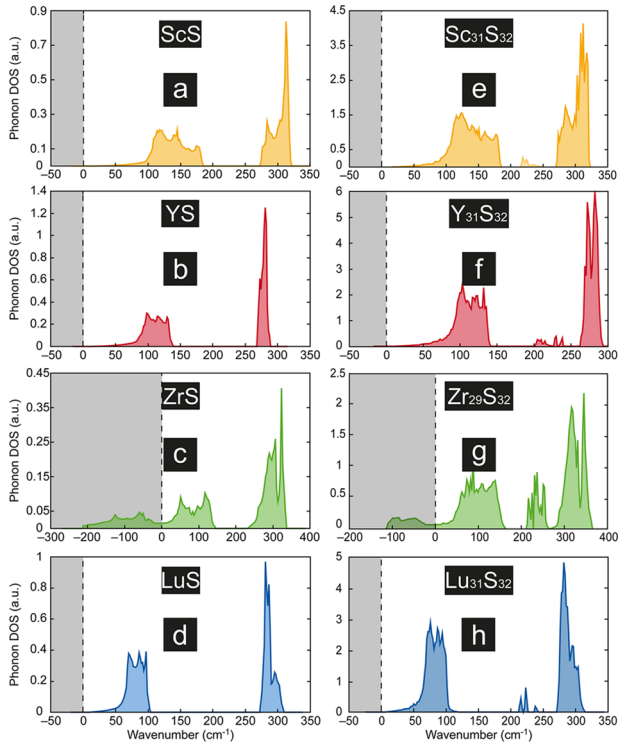

Figure 2. Phonon densities-of-states (DOS) curves of (a) ScS, (b) YS, (c) ZrS, (d) LuS, (e) $Sc_{31}S_{32}$, (f) $Y_{31}S_{32}$, (g) $Zr_{29}S_{32}$, and (h) $Lu_{31}S_{32}$: negative values of the wavenumbers (shaded in gray) correspond to imaginary modes, which typically point to a dynamically unfavorable situation for a given material.

Under consideration of the differences between ΔH_f ($M_{32}S_{32}$) and ΔH_f ($M_{31}S_{32}$), the absence of dynamic instabilities for MS and $M_{31}S_{32}$ (M = Sc, Y, Lu) implies that the tendency to form the metal-deficient sulfide is rather influenced by subtle effects in the electronic (band) structures. An inspection of the phonon densities-of-states for the zirconium-containing sulfides, i.e., ZrS and $Zr_{29}S_{32}$ (Figure 2), shows that imaginary wavenumbers are evident for both sulfides, which, accordingly, should be dynamically unstable. Note that the phonon frequencies in ZrS correspond to more negative values than those in the zirconium-deficient $Zr_{29}S_{32}$. This outcome suggests that the incorporation of zirconium vacancies may alleviate the dynamic instability. In this context, it is also remarkable that the experimentally determined phase width of the zirconium sulfide spans a more metal-deficient existence range relative to the remaining sulfides (see above).

To examine the influence of vacancies on the dynamic stabilities of zirconium sulfides in more detail, the vibrational properties were also investigated for Zr_3S_4, which has been reported[43] to crystallize with a superstructure of the NaCl-type sulfide and is zirconium-poorer relative to the other zirconium

DOI: 10.1021/acsomega.9b02368
ACS Omega 2019, 4, 15721−15728

sulfides. An examination of the phonon DOS for Zr_3S_4 (Figure 3) shows that the phonon frequencies in Zr_3S_4 indeed

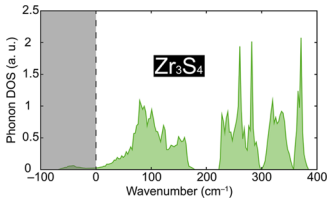

Figure 3. Phonon densities-of-states curve of Zr_3S_4: negative values of the wavenumbers (shaded in gray) correspond to imaginary modes.

correspond to less negative values than those in ZrS and $Zr_{29}S_{32}$. Accordingly, it may be inferred that the presence of vacancies in the crystal structures of the zirconium sulfides alleviates this dynamic instability. The existence of negative values in the phonon DOS of Zr_3S_4 still indicates that this material should be dynamically unstable. This result raises the question of whether this dynamic instability could also be reduced through adopting a different, but closely related type of structure;[48,49] yet, that prediction requires further explorations. To understand the tendencies to form the metal-deficient sulfides at the atomic level, we followed up with an analysis of the electronic band structures, densities-of-states, and projected crystal orbital Hamilton populations (pCOHP) for all sulfides.

Electronic Band Structures and Densities of States. An examination of the densities-of-states (DOS) curves for all sulfides (Figures 4 and 5) shows that the states close to the Fermi levels mostly originate from the M-d as well as S-p atomic orbitals (AOs). More precisely, the M-d states primarily reside in the energy regions around the Fermi levels, while the bands arising from the S-p AOs are located in energy regions below those ranges, which stem from the M-d states. Because a number of bands cross the Fermi level in each sulfide, all of the inspected sulfides should be metals. In the flat band/steep band scenario,[7,8] one would expect that these atomic orbitals contribute to flat bands as well as steep bands, which cross the Fermi levels of these rock salt-type sulfide-superconductors. Yet, an inspection of the electronic band structures shows that flat bands, which intersect the Γ-point in the electronic band structures of MS (M = Sc, Y, Zr), are positioned close to, but not at the Fermi levels in the respective sulfides. Notably, a maximum, which crosses the W-point in the electronic band structure of ZrS, is also located close to, but not at the Fermi level. In the case of LuS, a flat band crosses the Fermi level at the Γ-point. As pointed out by previous research,[19] the absence of flat bands at the Fermi levels in MS (M = Sc, Y, Zr) may lead to a discrepancy between the observed metal-to-superconductor-transitions and an anticipated flat band/steep band scenario. Previous research[16] on the electronic band structures of chalcogenide superconductors existing over certain homogeneity ranges, however, demonstrated that the electronic structures and, furthermore, positions of flat bands relative to the Fermi levels are influenced by the presence of vacancies in the crystal structures of the chalcogenides. Indeed, an inspection of the electronic band structures for the metal-deficient $M_{31}S_{32}$ (M = Sc, Y, Lu) and $Zr_{29}S_{32}$ indicates that flat bands cross the Fermi levels in these sulfides. Furthermore, an examination of the DOS curves for $M_{31}S_{32}$ (M = Sc, Y, Lu) and $Zr_{29}S_{32}$ shows that the Fermi levels fall at peaks of the DOS. In

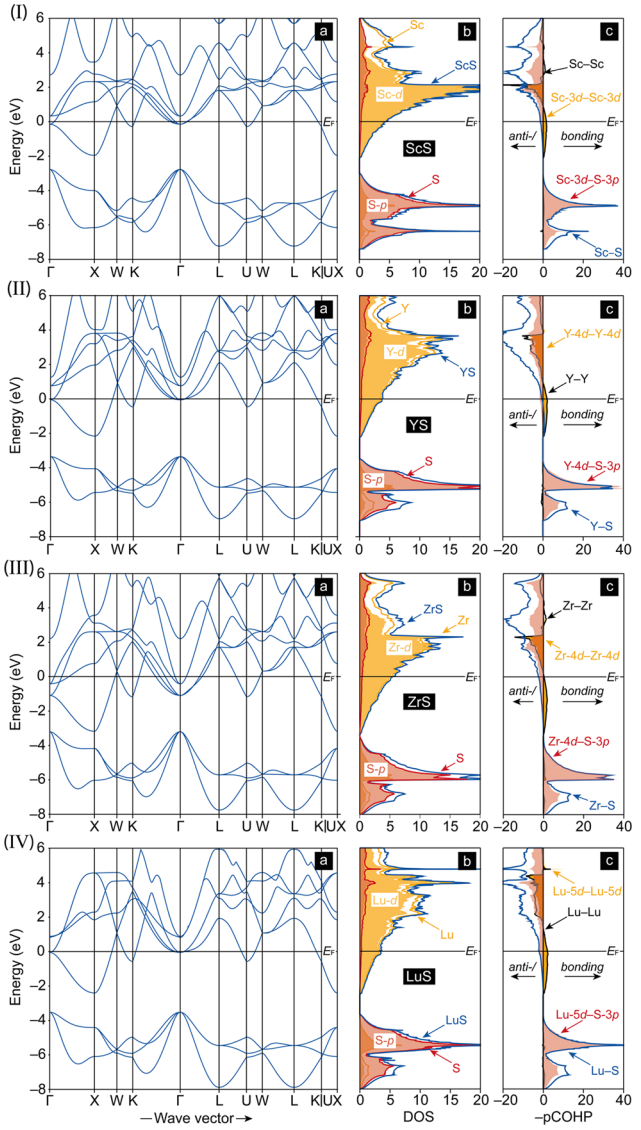

Figure 4. (a) Electronic band structures, (b) densities-of-states (DOS) curves, and (c) projected crystal orbital Hamilton population curves (pCOHP) of (I) ScS, (II) YS, (III) ZrS, and (IV) LuS: the Fermi levels, E_F, are represented by the black horizontal lines.

this connection, it should also be noted that the presence of flat bands at the Fermi level in a given material is typically related to electronic instabilities (see Introduction) such that the electronic situations encountered for $M_{31}S_{32}$ (M = Sc, Y, Lu) and $Zr_{29}S_{32}$ should be less favorable than those observed for MS (M = Sc, Y, Zr, Lu). Why, then, should the former sulfides be formed?

To answer this question, we followed up with a chemical bonding analysis for these sulfides. In this context, we also examined the prospect of M−M bonding interactions because the locations of the occupied M-d states at the Fermi levels may also imply that these orbitals interact via M−M bonds.

Bonding Analysis. A (chemical) bonding analysis for all sulfides was accomplished based on the projected crystal orbital Hamilton populations (pCOHP) and their respective integrated values (Figures 4 and 5). In the framework of the pCOHP approach that is a variant of the COHP technique, the bonding information is gained from the plane-wave-based computations (see Computational Details).

DOI: 10.1021/acsomega.9b02368
ACS Omega 2019, 4, 15721−15728

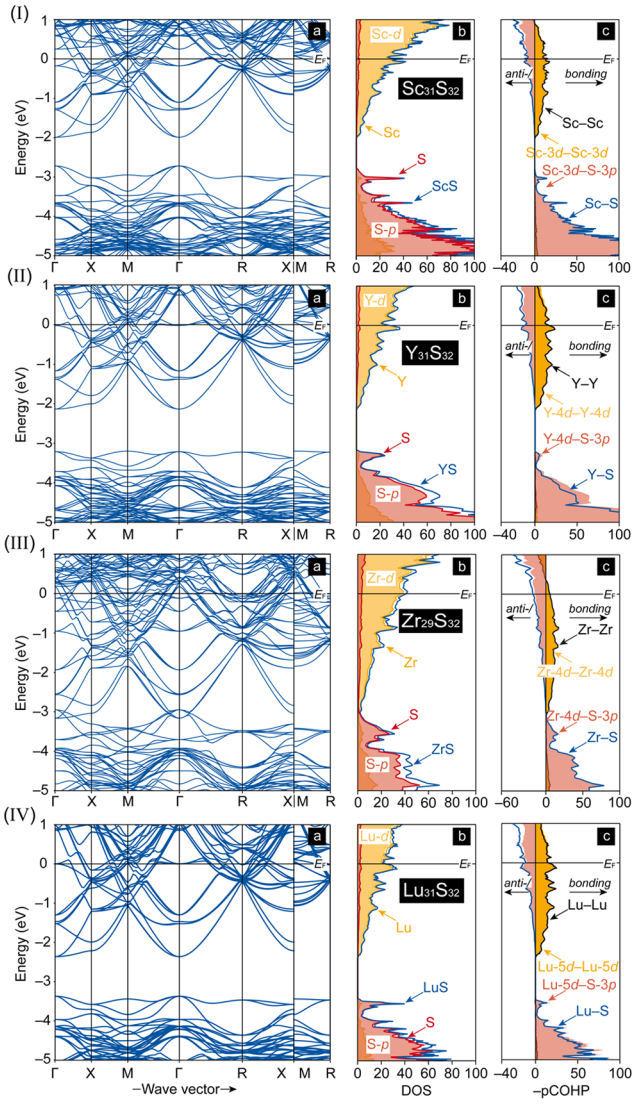

Figure 5. (a) Electronic band structures, (b) densities-of-states (DOS), and (c) projected crystal orbital Hamilton populations (pCOHP) curves of (I) $Sc_{31}S_{32}$, (II) $Y_{31}S_{32}$, (III) $Zr_{29}S_{32}$, and (IV) $Lu_{31}S_{32}$: the black horizontal lines represent the Fermi levels, E_F.

An examination of the −pCOHP curves for all sulfides reveals that the transition-metal−sulfide interactions near the Fermi levels stem essentially from contributions of the M-d and S-p atomic orbitals. The heteroatomic M−S interactions change from bonding to antibonding states below the Fermi levels in all sulfides and, hence, are of an antibonding nature at the Fermi levels. The antibonding M−S interactions are "counterbalanced" by bonding M−M interactions. The latter homoatomic interactions arise mainly from the M-d bands located around the Fermi levels. An integration of the heteroatomic M−S and homoatomic M−M interactions indicates net bonding characters for these interactions (see Table 2). Yet, how can these interactions affect the presence of vacancies and, furthermore, the chemical compositions of these sulfides?

To answer this question, we followed up with a closer examination of the −IpCOHP values for the sulfides. A direct comparison between the −IpCOHP values of compounds with dissimilar compositions cannot be made because the average electrostatic potential in each density functional theory-based computation is set to an arbitrary "zero" energy, whose relative position may vary from system to system.[9,50] In the lack of a true reference energy, the cumulative −IpCOHP/cell values, i.e., the sums of all negative IpCOHP/bond values for one particular type of nearest neighbor, interatomic interaction within one unit cell, were projected as percentages of the respective net bonding capabilities, a procedure that has been largely described elsewhere.[36,51]

A comparison of the negative integrated pCOHP values (−IpCOHP) for all inspected sulfides demonstrates that the −IpCOHP values of the heteroatomic M-d−S 3p interactions are larger than those related to the homoatomic M-d−M-d separations (Table 2). Because of such broad differences between the −IpCOHP values, the M-d−S 3p interactions have much larger percentage contributions to the net bonding capabilities than the homoatomic M-d−M-d interactions in all sulfides. Accordingly, this outcome suggests that the majority of the bonding interactions occurs between the M−S contacts beside minor, but evident M−M bonding, a circumstance that has also been encountered for certain reduced (divalent) rare-earth-metal halides[52] and transition-metal oxides.[53] A comparison between the percentage contributions of the rock salt-type sulfides and the corresponding metal-deficient species reveals that the percentages of the M-d−S 3p interactions are larger in the metal-deficient sulfides than in the respective (parental) non-metal-deficient sulfides. This result indicates that the occupations of antibonding M-d−S 3p states at the Fermi level in a given sulfide are reduced as the number of vacancies in the

Table 2. Average −IpCOHP/Bond Values, Cumulative −IpCOHP/Cell Values, and Percentage Contributions to the Respective Net Bonding Capabilities of Diverse Interactions in MS (M = Sc, Y, Zr, Lu), $M_{31}S_{32}$ (M = Sc, Y, Lu), and $Zr_{29}S_{32}$

interaction	Ave. −IpCOHP/bond	Cum. −IpCOHP/cell	%	interaction	Ave. −IpCOHP/bond	Cum. −IpCOHP/cell	%
	ScS ≡ $Sc_{32}S_{32}$				$Sc_{0.97}S$ ≡ $Sc_{31}S_{32}$		
Sc 3d−S 3p	0.8741	20.9777	86.72	Sc 3d−S 3p	0.8881	165.1856	87.46
Sc 3d−Sc 3d	0.1338	3.2117	13.28	Sc 3d−Sc 3d	0.1316	23.6933	12.54
	YS ≡ $Y_{32}S_{32}$				$Y_{0.97}S$ ≡ $Y_{31}S_{32}$		
Y 4d−S 3p	1.0665	25.5959	83.16	Y 4d−S 3p	1.0807	201.0076	83.98
Y 4d−Y 4d	0.2159	5.1818	16.84	Y 4d−Y 4d	0.2131	38.3508	16.02
	ZrS ≡ $Zr_{32}S_{32}$				$Zr_{0.91}S$ ≡ $Zr_{29}S_{32}$		
Zr 4d−S 3p	1.1381	27.3148	82.24	Zr 4d−S 3p	1.1967	208.2256	83.85
Zr 4d−Zr 4d	0.2459	5.9004	17.76	Zr 4d−Zr 4d	0.2571	40.1046	16.15
	LuS ≡ $Lu_{32}S_{32}$				$Lu_{0.97}S$ ≡ $Lu_{31}S_{32}$		
Lu 5d−S 3p	1.1743	28.1843	82.07	Lu 5d−S 3p	1.1901	221.3638	82.96
Lu 5d−Lu 5d	0.2565	6.1565	17.93	Lu 5d−Lu 5d	0.2526	45.4686	17.04

DOI: 10.1021/acsomega.9b02368
ACS Omega 2019, 4, 15721−15728

crystal structure of the respective sulfide increases. Notably, such a tendency has also been observed by previous research on the interdependence between the electronic structures of phase change materials and the presence of vacancies in their crystal structures.[54]

At this point, one may expect that the formations of the metal-deficient species are favored because of the aforementioned depletion of destabilizing, antibonding M−S states, which correspond to the largest percentages to the net bonding capabilities. Indeed, that conclusion is in accordance with previous[55] research, which implied that the presence of metal vacancies corresponds to an increase of metal cation−chalcogenide anion orbital mixing and, eventually, the stabilization of an entire defect (transition-metal chalcogenide) crystal structure. Yet, why do the nonmetal-deficient transition-metal sulfides exist? Actually, the differences between the percentage contributions of the M−S interactions in MS (M = Sc, Y, Zr, Lu) and those in the respective metal-deficient sulfides are rather small such that the latter rather tend to be preferred. Furthermore, electronically unfavorable situations have been identified for all metal-deficient sulfides because occupied flat bands are located at the Fermi levels in $M_{31}S_{32}$ (M = Sc, Y, Lu) and $Zr_{29}S_{32}$ (see above). Thus, it may be inferred that the interplay between the occupations of flat bands at the Fermi level, which typically signify electronic instabilities, and the populations of antibonding M-d−S 3p states appears to control the presence of vacancies in the crystal structures of these sulfides.

CONCLUSIONS

In the light of (computational) materials design, there is a need to understand the origins of vacancies in the crystal structures of compounds existing over certain homogeneity ranges because the electronic structure and, ultimately, the physical properties of such a material depend on the particular composition. In this connection, the origins of structural defects have been explored for the examples of rock salt-type sulfide-superconductors, i.e., MS (M = Sc, Y, Zr, Lu), by means of quantum-chemical techniques. Because the aforementioned sulfides have been reported to exist over certain homogeneity ranges, the vibrational properties, electronic band structures, and nature of bonding were examined for MS (M = Sc, Y, Zr, Lu) as well as $M_{31}S_{32}$ (M = Sc, Y, Lu) and $Zr_{29}S_{32}$. The crystal structures of the latter sulfides were derived from those of the former sulfides, but comprise fewer metal atoms than the rock salt-type sulfides in accordance with the experimentally determined crystal structures and phase widths.

An examination of the vibrational properties revealed that MS and $M_{31}S_{32}$ (M = Sc, Y, Lu) are dynamically stable such that the formation of a given metal-deficient sulfide appears to be controlled by effects in the electronic (band) structures. In the case of the zirconium-containing sulfides, an inspection of the phonon densities-of-states showed that the presence of vacancies apparently alleviates a dynamic instability for that sulfide; yet, the negative values of the phonon frequencies indicate that all of the inspected zirconium sulfides should be dynamically unstable. In the electronic band structures of LuS, $M_{31}S_{32}$ (M = Sc, Y, Lu), and $Zr_{29}S_{32}$, the Fermi levels are crossed by flat bands, which are in good agreement with a flat band/steep band scenario expected for superconductors. Because the populations of flat bands at the Fermi level in a given material are indicative of an electronically unfavorable situation, the nature of bonding was examined for all sulfides to explain the trends for the formation of the metal-deficient sulfides.

A bonding analysis based on the −pCOHP approach demonstrated that the bonding situations in all sulfides are dominated by strong M-d−S 3p bonding interactions, besides minor, but evident, M-d−M-d interactions. The M-d−S 3p interactions are antibonding around the Fermi levels, and the occupations of these antibonding states are reduced as the metal contents of the sulfides decrease. Accordingly, it may be concluded that the subtle interplay between the populations of flat bands and antibonding M-d−S 3p states at the Fermi levels appears to control the presence of vacancies in the crystal structures of the sulfides.

AUTHOR INFORMATION

Corresponding Author

*E-mail: simon.steinberg@ac.rwth-aachen.de.

ORCID

Simon Steinberg: 0000-0001-8022-7018

Author Contributions

J.S. conducted the first-principles-based computations, while S.S. supervised the project and prepared the initial draft of the manuscript. The manuscript was written with contributions from all the authors, who have approved the final version of the manuscript.

Funding

This work was supported by the Fonds der Chemischen Industrie e.V. (VCI), Frankfurt a. M. through a Liebig-stipend to S.S.

Notes

The authors declare no competing financial interest.

ACKNOWLEDGMENTS

The authors wish to thank Prof. Dr. R. Dronskowski for valuable advice as well as the allocation of the computer cluster of the Chemistry Department of RWTH Aachen, and, furthermore, the IT Center of RWTH Aachen for the computational resources (JARA-HPC project jara0167).

REFERENCES

(1) Zaanen, J.; Chakravarty, S.; Senthil, T.; Anderson, P.; Lee, P.; Schmalian, J.; Imada, M.; Pines, D.; Randeria, M.; Varma, C.; Vojta, M.; Rice, M. Towards a complete theory of high T_c. *Nat. Phys.* **2006**, *2*, 138−143.

(2) Bardeen, J.; Cooper, L. N.; Schrieffer, J. R. Theory of Superconductivity. *Phys. Rev.* **1957**, *108*, 1175−1204.

(3) Ginzburg, V. L.; Landau, L. D. On the Theory of Superconductivity. In *On Superconductivtiy and Superfluidity*; Ginzburg, V. L., Ed.; Springer-Verlag: Berlin, Germany, 2009; pp 113−137.

(4) Bednorz, J. G.; Müller, K. A. Possible high Tc superconductivity in the Ba−La−Cu−O system. *Z. Phys. B: Condens. Matter* **1986**, *64*, 189−193.

(5) Markiewicz, R. S. A SURVEY OF THE VAN HOVE SCENARIO FOR HIGH-T_c SUPERCONDUCTIVITY WITH SPECIAL EMPHASIS ON PSEUDOGAPS AND STRIPED PHASES. *J. Phys. Chem. Solids* **1997**, *58*, 1179−1310.

(6) Gabovich, A. M.; Voitenko, A. I.; Ausloos, M. Charge- and spin-density waves in existing superconductors: competition between Cooper pairing and Peierls or excitonic instabilities. *Phys. Rep.* **2002**, *367*, 583−709.

(7) Simon, A. Superconductivity and Chemistry. *Angew. Chem., Int. Ed.* **1997**, *36*, 1788−1806.

(8) Simon, A. Superconductivity — a source of surprises. *Solid State Sci.* **2005**, *7*, 1451−1455.

DOI: 10.1021/acsomega.9b02368
ACS Omega 2019, 4, 15721−15728

(9) Dronskowski, R. *Computational Chemistry of Solid State Materials*; WILEY-VCH: Weinheim, Germany, 2007.
(10) Johrendt, D.; Felser, C.; Jepsen, O.; Andersen, O. K.; Mewis, A.; Rouxel, J. LMTO Band Structure Calculations of $ThCr_2Si_2$-Type Transition Metal Compounds. *J. Solid State Chem.* **1997**, *130*, 254−265.
(11) Provino, A.; Steinberg, S.; Smetana, V.; Kulkarni, R.; Dhar, S. K.; Manfrinetti, P.; Mudring, A.-V. Gold-rich $R_3Au_7Sn_3$: establishing the interdependence between electronic features and physical properties. *J. Mater. Chem. C* **2015**, *3*, 8311−8321.
(12) Schmitt, D. C.; Drake, B. L.; McCandless, G. T.; Chan, J. Y. Targeted Crystal Growth of Rare Earth Intermetallics with Synergistic Magnetic and Electrical Properties: Structural Complexity to Simplicity. *Acc. Chem. Res.* **2015**, *48*, 612−618.
(13) Miller, G. J. The "Coloring Problem" in Solids: How it Affects Structure, Composition and Properties. *Eur. J. Inorg. Chem.* **1998**, *1998*, 523−536.
(14) Tarascon, J. M.; Greene, L. H.; McKinnon, W. R.; Hull, G. W.; Geballe, T. H. Superconductivity at 40 K in the Oxygen-Defect Perovskites $La_{2-x}Sr_xCuO_{4-y}$. *Science* **1987**, *235*, 1373−1376.
(15) Oyanagi, H.; Ihara, H.; Matsubara, T.; Tokumoto, M.; Matsushita, T.; Hirabayashi, M.; Murata, K.; Terada, N.; Yao, T.; Iwasaki, H.; Kimura, Y. Valence Study of Orthorhombic and Tetragonal $Ba_2YCu_3O_y$: The Role of Oxygen Vacancies in High-T_c Superconductivity. *Jpn. J. Appl. Phys.* **1987**, *26*, L1561−L1564.
(16) Novikov, D. L.; Freeman, A. J. Van Hove singularities and the role of doping in the stabilization, synthesis and superconductivity of $HgBa_2Ca_{n-1}Cu_nO_{2n+2+\delta}$. *Phys. C* **1993**, *216*, 273−283.
(17) Hulliger, F.; Hull, G. W. Superconductivity in rocksalt-type compounds. *Solid State Commun.* **1970**, *8*, 1379−1382.
(18) Moodenbaugh, A. R.; Johnston, D. C.; Viswanathan, R.; Shelton, R. N.; DeLong, L. E.; Fertig, W. A. Superconductivity of Transition Metal Sulfides, Selenides and Phosphides with the NaCl Structure. *J. Low Temp. Phys.* **1978**, *33*, 175−203.
(19) Fries, K. S.; Steinberg, S. Fermi-Level Characteristics of Potential Chalcogenide Superconductors. *Chem. Mater.* **2018**, *30*, 2251−2261.
(20) Hahn, H.; Harder, B.; Mutschke, U.; Ness, P. Zur Kristallstruktur einiger Verbindungen und Phase des Systems Zirkon/Schwefel. *Z. Anorg. Allg. Chem.* **1957**, *292*, 82−96.
(21) Blöchl, P. E. Projector augmented wave method. *Phys. Rev. B: Condens. Matter Mater. Phys.* **1994**, *50*, 17953−17979.
(22) Kresse, G.; Marsman, M.; Furthmüller, J. Vienna Ab Initio Simulation Package (VASP), The Guide. In *Computational Materials Physics*; Faculty of Physics, Universität Wien: Vienna, Austria, 2014.
(23) Kresse, G.; Furthmüller, J. Efficiency of ab-initio total energy calculations for metals and semiconductors using a plane-wave basis set. *Comput. Mater. Sci.* **1996**, *6*, 15−50.
(24) Kresse, G.; Furthmüller, J. Efficient iterative schemes for ab initio total-energy calculations using a plane-wave basis set. *Phys. Rev. B: Condens. Matter Mater. Phys.* **1996**, *54*, 11169−11186.
(25) Kresse, G.; Hafner, J. Ab initio molecular dynamics for liquid metals. *Phys. Rev. B: Condens. Matter Mater. Phys.* **1993**, *47*, 558−561.
(26) Kresse, G.; Joubert, D. From ultrasoft pseudopotentials to the projector augmented-wave method. *Phys. Rev. B: Condens. Matter Mater. Phys.* **1999**, *59*, 1758−1775.
(27) Perdew, J. P.; Burke, K.; Ernzerhof, M. Generalized gradient approximation made simple. *Phys. Rev. Lett.* **1996**, *77*, 3865−3868.
(28) Setyawan, W.; Curtarolo, S. High-throughput electronic band structure calculations: Challenges and tools. *Comput. Mater. Sci.* **2010**, *49*, 299−312.
(29) Ong, S. P.; Richards, W. D.; Jain, A.; Hautier, G.; Kocher, M.; Cholia, S.; Gunter, D.; Chevrier, V. L.; Persson, K. A.; Ceder, G. Python Materials Genomics (pymatgen): A robust, open-source python library for materials analysis. *Comput. Mater. Sci.* **2013**, *68*, 314−319.
(30) Parlinski, K.; Li, Z. Q.; Kawazoe, Y. First-Principles Determination of the Soft Mode in Cubic ZrO_2. *Phys. Rev. Lett.* **1997**, *78*, 4063−4066.
(31) Togo, A.; Oba, F.; Tanaka, I. First-principles calculations of the ferroelastic transition between rutile-type and $CaCl_2$-type SiO_2 at high pressures. *Phys. Rev. B: Condens. Matter Mater. Phys.* **2008**, *78*, No. 134106.
(32) Deringer, V. L.; Stoffel, R. P.; Wuttig, M.; Dronskowski, R. Vibrational properties and bonding nature of Sb_2Se_3 and their implications for chalcogenide materials. *Chem. Sci.* **2015**, *6*, 5255−5262.
(33) Göbgen, K. C.; Steinberg, S.; Dronskowski, R. Revisting the Si-Te System: $SiTe_2$ Finally Found by Means of Experimental and Quantum-Chemical Techniques. *Inorg. Chem.* **2017**, *56*, 11398−11405.
(34) Clark, W. P.; Steinberg, S.; Dronskowski, R.; McCammon, C.; Kupenko, I.; Bykov, M.; Dubrovinsky, L.; Akselrud, L. G.; Schwarz, U.; Niewa, R. High-Pressure NiAs-Type Modification of FeN. *Angew. Chem., Int. Ed.* **2017**, *56*, 7302−7306.
(35) Dronskowski, R.; Blöchl, P. E. Crystal Orbital Hamilton Populations (COHP). Energy-Resolved Visualization of Chemical Bonding in Solids Based on Density-Functional Calculations. *J. Phys. Chem.* **1993**, *97*, 8617−8624.
(36) Steinberg, S.; Dronskowski, R. The Crystal Orbital Hamilton Population (COHP) Method as a Tool to Visualize and Analyze Chemcial Bonding in Intermetallic Compounds. *Crystals* **2018**, *8*, 225.
(37) Deringer, V. L.; Tchougréeff, A. L.; Dronskowski, R. Crystal Orbital Hamilton Population (COHP) Analysis As Projected from Plane-Wave Basis Sets. *J. Phys. Chem. A* **2011**, *115*, 5461−5466.
(38) Maintz, S.; Deringer, V. L.; Tchougréeff, A. L.; Dronskowski, R. Analytic Projection From Plane-Wave and PAW Wavefunctions and Application to Chemical-Bonding Analysis in Solids. *J. Comput. Chem.* **2013**, *34*, 2557−2567.
(39) Maintz, S.; Deringer, V. L.; Tchougréeff, A. L.; Dronskowski, R. LOBSTER: A Tool to Extract Chemical Bonding from Plane-Wave Based DFT. *J. Comput. Chem.* **2016**, *37*, 1030−1035.
(40) Eck, B. *wxDragon 2.1.2*; RWTH Aachen University: Aachen, Germany, 2017.
(41) Johnston, D. C.; Moodenbaugh, A. $Zr_{3+x}S_4$: A NEW SUPERCONDUCTING BINARY SULFIDE. *Phys. Lett. A* **1972**, *41*, 447−448.
(42) Moodenbaugh, A. R.; Johnston, D. C.; Viswanathan, R. Super conductivity in two NaCl structure compounds: α-ZrP and ScS_{1+x}. *Mater. Res. Bull.* **1974**, *9*, 1671−1675.
(43) Stocks, K.; Eulenberger, G.; Hahn, H. Darstellung und Kristallstruktur der Phasen Zr_3S_4 und Hf_3S_4. *Z. Anorg. Allg. Chem.* **1970**, *374*, 318−325.
(44) Dismukes, J. P.; White, J. G. The Preparation, Properties, and Crystal Structures of Some Scandium Sulfides in the Range Sc_2S_3−ScS. *Inorg. Chem.* **1964**, *3*, 1220−1228.
(45) Franzen, H. F.; Hariharan, A. V. An X-Ray Photoelectron Study of Nonstoichiometric Lutetium Monosulfides. *J. Solid State Chem.* **1978**, *26*, 189−193.
(46) Stoffel, R. P.; Wessel, C.; Lumey, M.-W.; Dronskowski, R. Ab Initio Thermochemistry of Solid-State Materials. *Angew. Chem., Int. Ed.* **2010**, *49*, 5242−5266.
(47) Stoffel, R. P.; Dronskowski, R. Lattice Dynamics and Thermochemistry of Solid-State Materials from First-Principles Quantum-Chemical Calculations. In *Handbook of Solid State Chemistry*; Dronskowski, R.; Kikkawa, S.; Stein, A., Eds.; Wiley-VCH GmbH & Co KGaA, 2017; pp 491−526.
(48) McTaggart, F. K.; Wadsley, A. D. The sulphides, selenides, and tellurides of titanium, zirconium, hafnium, and thorium I. Preparation and characterization. *Aust. J. Chem.* **1958**, *11*, 445−457.
(49) Nguyen, T.-H.; Franzen, H.; Harmon, B. N. The electronic structure of zirconium monosulfide. *J. Chem. Phys.* **1980**, *73*, 425−437.
(50) Börnsen, N.; Meyer, B.; Grotheer, O.; Fähnle, M. E_{cov} − a new tool for the analysis of electronic structure data in a chemical language. *J. Phys.: Condens. Matter* **1999**, *11*, L287−L293.

DOI: 10.1021/acsomega.9b02368
ACS Omega 2019, 4, 15721−15728

(51) Gladisch, F. C.; Steinberg, S. Revealing Tendencies in the Electronic Structures of Polar Intermetallic Compounds. *Crystals* **2018**, *8*, 80.
(52) Gerlitzki, N.; Meyer, G.; Mudring, A.-V.; Corbett, J. D. Praseodymium diiodide, PrI_2, revisited by synthesis, structure determination and theory. *J. Alloys Compd.* **2004**, *380*, 211−218.
(53) Burdett, J. K.; Hughbanks, T. NbO and TiO: Structural and Electronic Stability of Structures Derived from Rock Salt. *J. Am. Chem. Soc.* **1984**, *106*, 3101−3113.
(54) Wuttig, M.; Lüsebrink, D.; Wamwangi, D.; Wełnic, W.; Gilleßen, M.; Dronskowski, R. The role of vacancies and local distortions in the design of new phase-change materials. *Nat. Mater.* **2007**, *6*, 122−128.
(55) Burdett, J. K.; Mitchell, J. F. Electronic Origin of Non-stoichiometry in Early-Transition-Metal Chalcogenids. *Chem. Mater.* **1993**, *5*, 1465−1473.

DOI: 10.1021/acsomega.9b02368
ACS Omega 2019, 4, 15721−15728